AIB

NEW MEASUREMENT OF THE $\pi \to \mu \nu \gamma$ DECAY

Giacomo Bressi[(a)], Giovanni Carugno[(b)], Simonetta Cerdonio[(d,e)], Enrico Conti[(b)], Anna T. Meneguzzo[(b,c)] and Dino Zanello[(e)]

(a) I.N.F.N. sez. di Pavia, Via U. Bassi 6, Pavia, Italy

(b) I.N.F.N. sez. di Padova, Via Marzolo 8, Padova, Italy

(c) Dipartimento di Fisica "G. Galilei", Università di Padova, via Marzolo 8, Padova, Italy

(d) Dipartimento di Fisica, Università di Roma "La Sapienza", P.le A. Moro 2, Roma, Italy

(e) I.N.F.N. sez. di Roma I, P.le A. Moro 2, Roma, Italy

Preprint DFPD 97/EP/43

Submitted to Nucl. Phys. B.

SW9807

UNIVERSITÀ DEGLI STUDI DI PADOVA

DIPARTIMENTO DI FISICA "GALILEO GALILEI"

ISTITUTO NAZIONALE DI FISICA NUCLEARE

SEZIONE DI PADOVA

Via Marzolo, 8 - 35131 PADOVA (ITALIA)

NEW MEASUREMENT OF THE $\pi \to \mu\nu\gamma$ DECAY

Giacomo Bressi [a], Giovanni Carugno [b], Simonetta Cerdonio [d,e], Enrico Conti [b,1], Anna T. Meneguzzo [b,c] and Dino Zanello [e]

[a] *I.N.F.N. Sez. di Pavia, Via U. Bassi 6, Pavia, Italy*

[b] *I.N.F.N. Sez. di Padova, Via Marzolo 8, Padova, Italy*

[c] *Dipartimento di Fisica "G. Galilei", Università di Padova, Via Marzolo 8, Padova, Italy*

[d] *Dipartimento di Fisica, Università di Roma "La Sapienza", P.le A. Moro 2, Roma, Italy*

[e] *I.N.F.N. Sez. di Roma I, P.le A. Moro 2, Roma, Italy*

Abstract

We have measured the branching ratio of the radiative decay $\pi \to \mu\nu\gamma$. The energies of the gamma-ray and of the muon were both measured and the Dalitz-plot distribution of the decay was obtained.

The data agree well with the theoretical prediction (QED internal bremsstrahlung) down to a γ-ray energy of 1 MeV. The discrepancy reported in a previous experiment is not confirmed.

PACS numbers: 13.20.Cz, 14.40.Aq, 13.40.Ks

Keywords: Pion radiative decay; QED inner bremsstrahlung

1 Introduction

Although QED is a well-established theory, there appears from time to time experimental evidence (see for example [1–3]) pointing to an excess of "low-energy" gamma rays in different kinds of processes. In 1958 Castagnoli and Muchnik [4] suggested the possibility of a similar problem in the decay

$$\pi^+ \to \mu^+\nu\gamma \qquad (1)$$

[1] Corresponding author. Tel.: +39 49 8277071; fax: +39 49 8277102; e-mail: conti@pd.infn.it

Their evidence is indirect. Working with nuclear emulsions they brought pions to rest and measured the muon range. In a number of cases (about 10^{-4} of the total) the muon range was shorter than the one expected for the two-body decay $\pi \to \mu\nu$. They interpreted those events as due to reaction (1).

They measured the branching ratio of (1) as a function of the muon kinetic energy T_μ. For $T_\mu \leq 3.4$ MeV they agree with the QED theoretical prediction but for $T_\mu \leq 3.6$ MeV their experimental branching ratio is 4 times higher than QED. $T_\mu = 3.6$ MeV corresponds to a 1.2 MeV effective cutoff on the γ energy. Since 1958 these results were never checked, nor were the gamma and the muon energy spectra ever measured.

In this paper we present results from the experiment RAPID (RAdiative PIon Decay), run at the Paul Scherrer Institute (Villigen, CH), where both the muon and gamma energies were measured for events of reaction (1). We observe no discrepancy with QED down to $E_\gamma = 1$ MeV.

In Sect.2 the theoretical aspects of the decay are briefly summarized. Sect.3 presents the experimental apparatus and method. The run and data taking are described in Sect.4, the trigger in Sect.5 and the timing procedure in Sect.6. The calibration of the silicon detector and the determination of the beam momentum are the argument of Sect.7. Sect.8 deals with the data analysis. The fit procedure and results are presented in Sect.9. Our conclusions are in Sect.10.

2 Theory

The $\pi \to \mu\nu\gamma$ decay is due to the contribution of three Feynman diagrams. The first two describe the QED internal bremsstrahlung (IB) process, namely, the emission of the photon by the charged pion and muon lines. The third is the structure dependent term (SD), which arises because the photon can be emitted directly from the decay vertex due to the composite nature of the pion. It is however well known that in the process (1) the SD term is strongly suppressed with respect to IB in all the phase space. Therefore, the photon emission in the decay (1) can be considered as a pure QED process.

The differential decay amplitude is express in terms of the two adimensional variables $x = 2E_\gamma/M_\pi$ and $y = 2E_\mu/M_\pi$, where E_γ and E_μ are respectively the total gamma and muon energy and M_π is the pion mass. The general formula has been calculated in [5,6]:

$$\frac{1}{\Gamma(\pi \to \mu\nu)} \frac{d^2\Gamma}{dxdy} = A_{IB}F_{IB}(x,y) + A_{SD}F_{SD}(x,y) + A_{INT}F_{INT}(x,y)$$

The first term of the sum is the QED IB term, the second is the SD term and the third is the IB-SD interference. The last two terms are completely negligible in our case, so that the formula reduces to

$$\frac{1}{\Gamma(\pi \to \mu\nu)} \frac{d^2\Gamma}{dxdy} = A_{IB} F_{IB}(x,y) \tag{2}$$

where

$$A_{IB} = \frac{\alpha}{2\pi} \frac{1}{(1-r^2)^2}$$

$$F_{IB}(x,y) = \frac{1-y+r^2}{x^2(x+y-1-r^2)} \left[x^2 + 2(1-x)(1-r^2) - \frac{2xr^2(1-r^2)}{x+y-1-r^2} \right] \tag{3}$$

$r = m_\mu/M_\pi$ and m_μ is the muon mass.

The limits on the x and y range (with a massless neutrino) are:

$$2r \leq y \leq 1+r^2$$

$$1 - \frac{y}{2} - \frac{1}{2}\sqrt{y^2-4r^2} \leq x \leq 1 - \frac{y}{2} + \frac{1}{2}\sqrt{y^2-4r^2}$$

In terms of energies, $0 \leq E_\gamma \leq 29.79$ MeV, $0 \leq T_\mu \leq 4.12$ MeV. The gamma and muon spectra and the branching ratio diverge as $x \to 0$ and $y \to 1+r^2$. Natural cutoffs are the detection thresholds. In our case the threshold is set by the gamma detector.

3 Experimental method and setup

The goal of the experiment is to measure the energy of both muon and gamma coming from reaction (1) in order to obtain not only the branching ratio but also the full two-dimensional distribution.

The layout of the experimental setup is shown in fig.1.

The incoming pion is first detected by a fast CF_4 gas scintillator counter (for good timing), then slowed down and brought to rest in a silicon pad telescope. The decay γ is detected and measured in a liquid xenon Time Projection Chamber (TPC). The xenon scintillation light is used for triggering.

The silicon telescope (ST) measures the sum of the energies of the incoming pion and of the decay muon. The μ kinetic energy is obtained by subtracting the known energy of the pion.

A substantial physical background can be caused by the muon decays (from the chain $\pi \rightarrow \mu\nu, \mu \rightarrow e\nu\bar{\nu}(\gamma)$) occurring within the trigger coincidence time. For this reason the silicon system was enclosed in a box of plastic scintillators with the purpose of vetoing the positrons.

The CF_4 gas scintillation detector is housed in a box (5x5x5 cm^3) covered with thin aluminized mylar (100 μm) and seen on one side by a 3 inch MgF_2 window PM. The CF_4 gas is fluxed through the box at a rate of 10 cm^3 (NPT) per minute. The trigger efficiency for pions was higher than 95 %. Due to the different energy loss in the gas, the CF_4 detector was insensitive to the positrons.

The silicon telescope consists of 10 silicon detectors 5x5 cm^2, 500 μm thick. The anode of each detector is segmented in 50 strips, 1 mm wide, while the cathode is a single electrode. The strip direction is placed alternatively in two perpendicular directions. The ST is divided in two groups: the first is composed of two pads (for beam definition) and is separated by about 8 cm from the second group, composed of the remaining elements. The distance between two adjacent elements is 2 mm. The silicon detectors are housed in a 50 μm copper box acting as electromagnetic shield. The entrance window is a 25 μm aluminized mylar.

The readout chain of the ST is essentially based on the electronics developed for the DELPHI electromagnetic calorimeter [7]. It consists of a low-noise charge preamplifier, a shaping amplifier with a sample-and-hold circuit and a multiplexed 12 bits ADC. The shaping time τ_{shap} is 1.8 μs.

The hybrid charge preamplifiers [8] are situated in two copper boxes acting as a Faraday cage. Silicon detectors and preamplifier boxes are connected with multilayer kapton flat cables, 1 metre long.

The hybrid shapers [9] are mounted on fastbus-like boards, which also contain the analog multiplexers, the ADC and the control logic. The ADC data are read by a custom VME CPU [10], based on a Motorola DSP 56001, linked to the shaper-ADC boards via an interface board.

A 50 MeV/c π^+ stops and decays mainly in silicon nr.5 and the decay μ^+ reaches at most silicon nr.4 or 6. Silicon pads from 7 to 10 are not used for energy measurement but they were important for beam muon and positron contamination study and rejection. In particular silicon nr.9 enters directly in the trigger logic in order to reject beam muons. We used the cathode signal for the $\pi + \mu$ energy measurement and the strip signal to define the fiducial

volume for the pion decay region.

The TPC, its readout electronics and acquisition system were described in detail elsewhere [11]. We recall here only the features that have an interest in the analysis. The γ energy was measured by means of the ionization charge produced in the active volume of the TPC and collected by 12 anodes. The xenon scintillation light, used for triggering and timing, was detected by a system of 12 PM's (UVPM). All anode and PM signals were digitized and recorded for further analysis.

The TPC response was calibrated with the help of radioactive sources [12]. The minimum detectable gamma energy, measured by mean of the ionization charge, is 230 keV. The minimum energy seen by the PM's used in the trigger is 170 keV. The energy resolution is parameterized as

$$\frac{\sigma(E_\gamma)}{E_\gamma} = \frac{7\%}{\sqrt{E_\gamma}} \oplus \frac{0.14MeV}{E_\gamma}$$

where E_γ is in MeV and $\oplus$ indicates a quadratic sum.

The acceptance of the TPC, which includes also the trigger efficiency, is reported in fig.2.

The plastic scintillators (NE112) were 5 mm thick. The inefficiency (1-ϵ_{veto}) for each of the elements of the box was measured in a positron beam. Measurements were done in three different position for each element. The overall inefficiency was 0.5%. The presence of an entrance hole for the beam particles in the front scintillator introduces a geometrical inefficiency $g \approx 10^{-2}$. The veto signals were also fed into the fast ADC waveform digitizer (the same used for the TPC signals) so that the time sequence of the veto counters was also registered although with a poor time resolution (the ADC clock was 200 ns).

4 Beam and Run

The experiment was carried out at the P.S.I. laboratory in the experimental area πE1.

The pion beam is generated by the interaction of a 590 MeV primary proton beam with a Cu target.

At the selected beam momentum (nominal value = 50 MeV/c), the beam contains only a little fraction of pions and mostly positrons and muons. The

following ratios were measured

$e^+/\pi^+ \approx 10^3, \mu^+/\pi^+ \approx 10.$

We used an electrostatic deflector mostly to reduce the huge number of positrons. The system formed by the electrostatic deflector and a set of two quadrupoles was placed just upstream the target region. The positrons were bent upward and dumped onto a lead slit. After separation, the measured ratios were

$e^+/\pi^+ \approx 10, \mu^+/\pi^+ \approx 1.$

Even with the separator on, positrons create electromagnetic showers in the materials they hit. With the beam on, the TPC UVPM counted approximately 100 kHz. A big lead shield, 30 cm thick, was placed between the deflector and the TPC to reduce this background. With the lead wall and beam on, the TPC rate was around 4-5 kHz. With the beam off, the counting rate was about 50 Hz.

The beam exits the beam pipe through a thin mylar window at about 30 cm from the stopping point.

The beam momentum byte $\Delta p/p$ could be set by means of a momentum slit. We operated at $\Delta p/p = 0.5\%$.

The rate of pions, at our typical beam intensity, was about 800/s. After a period of about six weeks for beam studies and detector calibration and timing, we took data for two weeks stopping more than 200 millions pions for the study of decay (1).

5 Trigger

The signature of the decay (1) is the detection of a photon in the TPC. The veto counter system prevents confusion between gammas and positrons from μ decays (the TPC does not distinguish γ's from e^+'s) and reduces the γ background from decay (5), as explained later. The presence of a stopped pion in the ST is given by the coincidence

$$S = CF_4 * S_1 * S_2 * S_5 * \overline{S_9}$$

where CF_4 is the signal from the CF_4 detector, used only for timing purposes (see below), and S_i is the signal of the i-th element of the ST. The thresholds of the silicon detectors were adjusted in order to obtain the maximum discrimination between pions and muons. The addition of silicon 9 in anticoincidence

improves the muon rejection.

Defined V as the logical OR of all the veto counters, PM_γ as the TPC trigger given by the UVPM, the experimental trigger was

$$T = S * PM_\gamma * \overline{V} \tag{4}$$

If Δ_{veto} is the veto gate, some muons from reaction (1) decay within this interval causing a trigger inefficiency. In our case $\Delta_{veto} = 300$ ns and the resulting trigger efficiency is $\eta \approx 0.9$.

A physical background comes from the muon radiative decay

$$\mu^+ \rightarrow e^+ \nu \overline{\nu} \gamma \tag{5}$$

whose branching ratio is $\approx 6 \cdot 10^{-2}$ [13]. Because of the geometrical and intrinsic inefficiency of the veto detector, some of these decays are not vetoed. The contamination c of such events is

$$c = (1 - \epsilon_{veto} + g)\frac{1}{\eta}\frac{BR(\mu \rightarrow e\nu\overline{\nu}\gamma)}{BR(\pi \rightarrow \mu\nu\ \gamma)}\left[1 - exp\left(-\frac{\Delta}{\tau_\mu}\right)\right]$$

where $\Delta = 200$ ns is the coincidence gate. Since $BR(\mu \rightarrow e\nu\overline{\nu}\gamma)/\ BR(\pi \rightarrow \mu\nu\ \gamma) \approx 10^2$, $c \approx 15\%$.

However another kind of events are triggered due to the veto inefficiency. These are the events of the decay chain $\pi \rightarrow \mu \rightarrow e$ when the muon decays within Δ and the positron is not detected by the veto. The ratio λ of these events with respect to those of decay (1) is

$$\lambda = \frac{1 - \epsilon_{veto}}{\eta BR(\pi \rightarrow \mu\nu\ \gamma)}\left[1 - exp\left(-\frac{\Delta}{\tau_\mu}\right)\right]$$

In our case $\lambda \approx 1.3$.

Both these spurious triggers were removed at the offline analysis level (see Sect.8) by the requirement that a positron must be detected by the veto within a certain time interval following the trigger.

The most serious source of background comes from accidental coincidences between a stopped pion and a background photon. The probability is high because of the high counting rate of the TPC (see Sect.4). The spectrum of these events has however been measured by triggering with a delayed coincidence $S * \overline{V} * (PM_\gamma * \overline{V})_{delayed}$. The delay was set to 30 μs. Therefore two kinds of triggers were accepted at the same time:

1) prompt triggers (4), which select either $\pi \rightarrow \mu\nu\gamma$ decays, or accidental $\pi - \gamma$ coincidences, or muon decays because of the veto inefficiency;
2) delayed triggers, which select only accidental $\pi - \gamma$ coincidences.

6 Timing

The separate elements that should be put in coincidence for the trigger were:

1) the silicon telescope;
2) the CF_4 counter;
3) the scintillator veto system;
4) the UVPM system.

From the hardware point of view they were independent and could not be brought all together in the beam line for easy timing.

The silicon pads have a large capacitance ($\approx$ 1 nF) hence the output of the charge amplifier has a long risetime. Therefore a better definition for the pion arrival time was obtained by adding the CF_4 detector. Its jitter was estimated by looking at the CF_4 signal on the oscilloscope triggered by the accelerator RF signal and turned out to be (2-3) ns.

The CF_4-veto delay time was determined by using the pions which were scattered by the silicon system onto the scintillators themselves.

The veto-UVPM delay was measured via the positron crossing a veto scintillator and entering the chamber.

The silicon telescope-UVPM timing was effected by utilizing the decay chain $\pi \rightarrow \mu \rightarrow e$ and looking at the positrons entering the TPC. We defined the silicon trigger S as $S = CF_4 * S_\pi$ ($S_\pi = S_1 * S_2 * S_5 * \overline{S_9}$). The S_π signal was formed at $400ns$ and the CF_4 one at $40ns$. We counted the number of coincidences $S * PM_\gamma$ versus the PM_γ delay. The PM_γ signal was formed at $100ns$. We reconstructed the decay curve of the muon. The result is shown in fig.3. The delay of the silicon trigger was measured to be $500ns$ with respect the PM_γ .

Due to the short pion lifetime, a systematic error of $\approx$ 30 ns would result in cutting out practically the whole signal. Therefore, in order to check the timing and efficiency of the trigger, a special run was dedicated to the detection of the rare decay $\pi^+ \rightarrow e^+\nu$ which has the same time properties and approximately the same branching ratio of (1). It is defined by an energetic positron (70 MeV) in the TPC and by a single peak in the silicon telescope corresponding to the pion kinetic energy.

The veto counter V_{TPC} facing the TPC was put in coincidence with the UVPM signal while the remaining veto counters V' were put in anticoincidence. For a better definition of the positron direction we placed another plastic scintillator (0.5x10x40 cm^3) V_{extra} in front of the TPC and perpendicular to V_{TPC}. The $\pi^+ \to e^+\nu$ trigger was therefore $CF_4 * S_\pi * V_{TPC} * V_{extra} * \overline{V'}$.

We stopped 80.92 millions π^+ and recorded 301325 triggers. Most of them were due to the chain $\pi \to \mu\nu, \mu \to e\nu\overline{\nu}$ with the μ decaying within the coincidence gate. The positron coming from this decay have a maximum energy of 50 MeV, while the silicon spectrum is a peak, sum of the pion and muon kinetic energies. Thus a cut on the silicon and the TPC energies separate the region of the $\pi \to e\nu$ with respect to the $\pi \to \mu \to e$ chain. The detailed analysis of the data (restricted to a sample of 58 millions stopped pions) is reported in [14]. Here we recall only the results. We selected positrons with energy higher than 40 MeV. In the $\pi \to e\nu$ zone of the silicon spectrum we found 98 ± 10 events. A Monte Carlo (MC) simulation was used to evaluate the background and the expected number of events. The expected number of background events is 24 ± 5 while the expected number of $\pi \to e\nu$ decays is 88 ± 15. The $\pi \to e\nu$ is therefore clearly detected, thus confirming the correctness of our trigger.

7 Calibration of the silicon telescope and determination of the beam momentum

The first six silicon pads were calibrated analyzing the shape of the spectrum of the energy deposited in each device by real events. Events were chosen from the delayed-trigger sample since in this case the decay μ is essentially monochromatic. Our procedure produces not only the calibration constants but estimates also the absolute beam momentum, whose nominal value was 50 MeV/c.

The deposited energy spectrum in each pad was compared to a MC simulation, in which the incident pion momentum was moved in 0.1 MeV/c steps.

In the MC code, the 10 silicon devices and the plastic scintillator box were simulated in all details. All the materials crossed by the beam (CF_4, mylar windows,...) were taken into account. The π^+ beam was generated with a monochromatic momentum p_{beam} and with a gaussian shaped geometrical spot. The width and the centre of the spot were determined from the experimental data of sil.1 and 2. The beam was in the centre of the silicon telescope with $\sigma_x \approx 7mm$ (from sil.1) and $\sigma_y \approx 17mm$ (from sil.2). The experimental trigger was reproduced. The $\pi \to \mu \to e$ decay chain was followed and the time of birth of each particle was computed. The pulse height for each silicon was computed considering the energy deposited by each particle and the

response curve of the silicon front-end electronics. The cuts nr. 1, 2, 4 and 5 described in Sect.8 were applied both to the simulated and experimental data. Their purpose is manly to suppress the contribution of the positron from the μ decay.

For each silicon device, the energy-to-ADC counts conversion factor G and the energy independent electronic noise σ_{sil} were the parameters of the fit. At each simulated beam momentum, the fit was performed with the minimum χ^2 method using the program MINUIT [15]. The chisquare χ^2_{TOT} is the sum of the minimum χ^2 of sil.1 to 6. The dependence of χ^2_{TOT} on p_{beam} is shown in fig.4. The minimum of χ^2_{TOT} is 155 for 148 degrees of freedom at $p_{beam} = 50.04$ MeV/c. The error on p_{beam} is 0.03 MeV/c. The values of G and σ_{sil} for each silicon at this beam momentum are therefore the parameters which describe the behaviour of the ST. Table I shows the fitted parameters. Fig.5 shows the energy distribution for the silicon elements 1-6 together with the fitted MC spectra.

Silicon nr.3 appears more noisy than the others. This was not surprising since its leakage current was ten times higher than the others.

The total $\pi + \mu$ kinetic energy measured in the ST was 12.23 MeV and its variance 0.20 MeV. The expected total $\pi + \mu$ kinetic energy is 12.8 MeV for our beam momentum. The difference is due to the pion energy loss in air, in the CF_4 detector and in the windows. Concerning the silicon energy resolution, the quadratic sum of the electronic noises yields 135 keV. The spread caused by the momentum byte is 85 keV. The remaining 120 keV are due to the energy straggling of the pion in the various materials crossed during its slowing down.

Since the specific energy loss dE/dx varies by about two orders of magnitude from about 0.3 keV/μm for positrons to about a few tens keV/μm for stopping pions and muons, we checked the linearity of the silicon response. We also used an α-source (on silicon 10) which releases 5.18 MeV in about 30 μm (average $dE/dx \approx 170$ keV/μm). In fig.6 the dependence of the ADC counts on the energy released in the silicon is plotted, showing the good linearity over almost three order of magnitude of the specific ionization.

8 Monte Carlo simulation and data analysis

In order to compare the experimental data with the theoretical QED predictions a MC program simulating the apparatus and the trigger was developed using the library program GEANT [16]. It was tuned by mean of radioactive γ-ray sources to reproduce the TPC behaviour and trigger acceptance, as described in [12]. The silicon and the veto parts were checked and tuned as

described in the previous section. The veto counter was supposed to have unit efficiency.

The muon and gamma energies coming from (1) were generated according to formulae (2) and (3). The energy threshold for the γ-ray was set to 100 keV, below the experimental threshold. The trigger (4) was reproduced with the appropriate thresholds for the TPC and the ST.

For what concerns the data, the waveforms of the 12 TPC anodes were elaborated according to the algorithm described in [12,17] to determine the total energy E_{TPC} released in the chamber. For the 12 UVPM signals, the time of each TPC trigger was determined for the successive rejection of the pile-up signals. Fig.7 shows a display of a TPC event as it appears at the analysis level.

Concerning the veto counters, the time T_1 when the veto box is hit for the first time after the trigger time $T_{trigger}$ was determined and the time difference $\Delta T_{veto} = T_1 - T_{trigger}$ was computed. The front and the back scintillators, which intercepted the beam positrons, were excluded because of their high occupancy probability. The distribution of ΔT_{veto} is shown in fig.8. ΔT_{veto} behaves as the sum of two exponential curves: $\Delta T_{veto} = A_1 exp(-t/\tau_1) + A_2 exp(-t/\tau_2)$. As expected, τ_1 turns out to be the muon lifetime. The second exponential curve is due to the beam particles (mainly positrons) which travel randomly near the triggered pions. τ_2 is therefore the average distance of the beam particles. Since $\tau_2 \approx 85\mu s$, this means that the total beam intensity on target was about 12 kHz.

Our experimental trigger selected those pions which decay in the silicon nr.5. The subsequent muon could cross at maximum one silicon detector, reaching the silicon nr.4 or nr.6. It is therefore sufficient to sum the energies from silicon nr.1 to nr.6 to get the total kinetic energy of the pion plus the muon, E_{SILI}.

The following data selection were performed for the silicon data:

1) events were rejected if at least one silicon device overflows;
2) to avoid that a part of the particle track should escape the detector we discarded events where a silicon strip close to the border is hit. The fiducial volume was restricted to 42x42 mm^2 (strips 4 to 46);
3) the energy released in each silicon detector is required to be greater than an appropriate cut, which is the minimum energy that a pion can loose, evaluated by the MC;
4) due to the shaping time of the silicon shaping amplifiers a fraction of the energy of the positrons from the muon decay could be summed in E_{SILI}. We must then reject those events when $\Delta T_{veto} \leq \tau_{shap}$.
5) Another selection uses the quantity ΔT_{veto} to reject the triggers due to the veto inefficiency. The cut $\Delta T_{veto} \leq 3\tau_\mu$ eliminates those spurious triggers,

requiring the presence of a decay positron within three muon lifetimes.

The data selections concerning the LXe chamber are:

6) pile-up rejection. Events were discarded if at least another TPC trigger occurs within ± 1 drift time of the chamber (32 μs);
7) the TPC anode signals were sometimes affected by a pick-up noise which prevents the measurement of the gamma energy (in ref. [12] we have called it "synchronous noise" because it affects several TPC channels simultaneously). Those events however could be recognized and discarded. The algorithm that recognizes the presence of this noise introduces also some loss of good events.

The above data selections were applied both to the experimental data (prompt and delayed triggers) and to the MC simulation data. Table II shows the data reduction ϕ_{exp} and ϕ_{MC} for each cut.

Even after the cut 5) a fraction of spurious triggers caused by the veto inefficiency survives (fig.8). The distribution of these background events was obtained by selecting the events with $\Delta T_{veto} \geq 100$ ADC clocks ($9\tau_\mu$). The correct 2-dim spectra are then obtained by subtracting this background, after proper normalization.

Fig.9 shows the Dalitz-plot distribution obtained after this procedure for prompt-trigger, delayed-trigger and MC events.

The MC simulation does not take into consideration losses induced by the TPC pile-up (due to the background radiation) and by the veto inefficiencies. We calculated the correction factor f_i for each cut to be applied to the MC data for the right normalization with respect the experimental data. Except for cut 5), $f_i = \phi^{(i)}_{exp}/\phi^{(i)}_{MC}$.

The cut 5) eliminates events of the experimental data that would not have been triggered in an "ideal" situation and that are not simulated by the MC. Hence the correction factor f_5 is unit.

9 Results

9.1 Spectra

Accidental triggers caused by environmental gammas constitute a large and non-eliminable background to the experiment. However the shape of this background is experimentally given by the delayed-trigger sample. The prompt-

trigger data sample is therefore fitted to a linear combination of the delayed-trigger spectrum plus the QED term. We defined a χ^2 as follows:

$$\chi^2 = \sum_i \frac{(N_i - \alpha N_i^{MC} - \beta N_i^{BKG})^2}{N_i + \alpha^2 N_i^{MC} + \beta^2 N_i^{BKG}}$$

where

i) α and β are free parameters obtained by the χ^2 minimization;
ii) N_i is the number of the prompt-trigger events in the i-th bin;
iii) N_i^{MC} is, in the same bin, the number of events predicted by QED modified by our MC to take into account acceptances and cuts;
iv) N_i^{BKG} is given by the delayed-trigger events, which we assume to represent the background.

The fitting is carried on in two dimensions in the E_{TPC}-E_{SILI} plane. Since the distribution is very steep, the binning has been adjusted by hand with the criterion that the bin content should in any case be at least 10 events.

The fit with $\alpha = 0$ assesses our sensitivity to the QED term.

The limits for E_{SILI} are $8.2 \leq E_{SILI} \leq 12.4$ MeV. They correspond to the kinematical limits for T_μ. More delicate is the choice for the minimum E_{TPC}. Our natural choice would be $\approx$ 250 keV, which is close to the MC estimate of our reconstruction threshold. However we know that around 0.5 MeV the background spectrum, which has been measured with an NaI detector, has a huge peak and we do not expect to have enough sensitivity for seeing the signal in this region (we shall comment on this point further down). For this reason we prefer to be conservative and assume for E_{TPC} the limits $1.0 \leq E_{TPC} \leq 30$ MeV.

The fit yields:

$$\alpha = (8.9 \pm 1.1) \cdot 10^{-3}, \beta = 0.991 \pm 0.024$$

with $\chi^2/\mathrm{DoF} = 95.6/101$ (fit probability 63.2%).

The fit with α fixed to 0 yields:

$\beta = 1.065 \pm 0.024$ but $\chi^2/DoF = 159.7/102$ with a fit probability $\approx 2 \cdot 10^{-4}$.

The conclusion is that the QED term is needed and provides a good fit to our data.

The gamma and muon spectra are obtained by subtracting the background

spectra, with weight β, from the prompt-trigger spectra. The results are shown in fig.10 together with the fitted MC spectra.

As a check we have also carried a fit extending the region of E_{TPC} down to 0.25 MeV. The fit is still successful with a $\chi^2/DoF = 142.5/138$, corresponding to a probability of 37%. However one can clearly see that, as expected, the number of QED events obtained by the fit in the region $0.25 \leq E_{TPC} \leq 1.0$ MeV is compatible with zero. This confirms that this region, due to the high background, does not carry much information.

9.2 Branching ratio

For the calculation of the branching ratio of (1) we must evaluate the total data acceptance. This is done by mean of the MC simulation. In the MC the cut on the γ-ray energy was 100 keV, below our detection thresholds. The total MC efficiency ϵ_{MC} is

$$\epsilon_{MC} = \frac{N_\gamma^{MC}}{N_\pi^{MC}} \left[\frac{BR(E_\gamma > 100keV)}{BR(E_\gamma > E_{cut})} \right]_{QED}$$

where N_γ^{MC} is the number of simulated events after all the cuts in the region of the E_{TPC}-E_{SILI} plane selected for the fit when N_π^{MC} pions are stopped and decay, $BR(E_\gamma > E_{cut})$ is the branching ratio for E_γ greater than the TPC energy cut and $BR(E_\gamma > 100keV)$ the branching ratio for the E_γ cut used in the MC. The two BR's are calculated by numerical integration of (2) and (3).

We obtain

$\epsilon_{MC} = 1.894 \cdot 10^{-2}$.

Then the relation between the number of QED triggers and the experimental branching ratio is

$$\alpha N_\gamma^{MC} = N_\pi \cdot BR(E_\gamma > E_{cut})_{exp} \cdot F \cdot \epsilon_{MC} \qquad (6)$$

where $F = \Pi_i f_i$ is a global reduction factor and the f_i's are found in Table II, N_π is the number of stopped pions and α is given by the fit described above. In (6) the trigger efficiency η does not appear because it is already included in ϵ_{MC}. With our numbers :

$F = 0.437$, $N_\pi = 207.4 \cdot 10^6$, $\alpha N_\gamma^{MC} = 335.2$,

the measured branching ratio is $\mathrm{BR}(E_\gamma > 1 \text{ MeV})_{exp} = 1.953 \cdot 10^{-4}$.

The statistical error comes only from the parameter α since the statistical errors on the other quantities in (6) are negligible.

The systematic error of the product $\epsilon_{MC} \cdot F$ must be evaluated. First of all, we verified that $\epsilon_{MC} \cdot F$ does not depend of the cut order. Two are the major sources of systematic errors. The first comes from the errors on the threshold detection for the TPC and UVPM signals used in the MC. The second comes from the transformation of the time interval ΔT_{veto} from seconds to ADC clock for the simulated data. This operation introduces an indetermination of ± 1 ADC clock. The other cuts do not contribute appreciably to the systematic error.

By varying the TPC and UVPM thresholds by one standard deviation, the product $\epsilon_{MC} \cdot F$ changes on the whole by 3.2%. The variation of ± 1 ADC clock causes a systematic difference of 8.6%. The corresponding standard deviation is $8.6\%/\sqrt{12} = 2.5\%$. The quadratic sum of these two errors yields a total systematic error equal to 4.0%. Thus our result is

$$BR(E_\gamma > 1MeV)_{exp} = 1.95 \cdot 10^{-4} \pm 12.2\%(stat) \pm 4.0\%(syst)$$

to be compared with the theoretical branching ratio $2.283 \cdot 10^{-4}$.

10 Conclusions

Our data agree well with the QED predictions, not only for what concerns the branching ratio but also in the Dalitz-plot distribution. The discrepancy reported in [4] is not confirmed. We wish to point out that, in comparison with [4], this experiment measured both the kinematical variables of decay (1), covering a somewhat wider range of the same variables.

Since in this experiment we are triggering on the presence of a gamma-ray, our result shows unambiguously that reaction (1) is described correctly by QED. Strictly speaking, though, we cannot state that our result is incompatible with what reported in [4], since they do not observe the γ-ray. However, for the two results to be compatible, one would have to assume that the excess of events reported in [4] does not come from decay (1).

Acknowledgements

The authors are specially indebted to R. Onofrio (Padova) for his continuous help during all the phases of the experiment and to A. Lanza (Pavia) for the setup of the silicon detector and related electronics. They are also very grateful to S. Ventura (Padova) and G. Boca (Pavia) for their presence during the data taking.

The authors would like to thank O. Barnaba and E. D'Uscio (Pavia), U. Beriotto, S. De Biasia, M. Nicoletto, R. Pedrotta and G. Salvato (Padova), M. Bertino (Roma), S. Marigo and N. Toniolo (Legnaro) for their skilful technical support.

The authors acknowledge R. Frosch, P. Gheno, R. Abela and the PSI staff for their help before and during run at PSI. They thank the PSI for its hospitality.

References

[1] S. Benerjee et al, Phys. Lett. **B305** (1993), 182
A. Belogianni et al., CERN PPE/96-145 (1996)

[2] J.J. Aubert et al., Phys. Lett. **B218** (1989), 248

[3] P.V. Chliapnikov et al., Phys. Lett. **B141** (1984), 276

[4] C. Castagnoli, M. Muchnik, Phys. Rev. **112** (1958), 1779

[5] S.G. Brown, S.A. Bludmann, Phys. Rev. **136** (1964), 1160

[6] D.E. Neville, Phys. Rev. **124** (1961), 2037

[7] P.Checchia et al., Nucl. Instr. and Meth. **A248** (1986), 317
P.Checchia et al., Nucl. Instr. and Meth. **A275** (1989), 49

[8] G. Barichello et al., Nucl. Instr. and Meth. **A254** (1987), 111

[9] I. Lippi et al., Nucl. Instr. and Meth. **A286** (1990), 243

[10] "CPU DSP56 and DSPbug 5.0", INFN Pavia, Servizio Elettronico
"Acquisizione VME per la scheda di readout FEMC", INFN Pavia, Servizio Elettronico

[11] G. Carugno et al., Nucl. Instr. and Meth. **A376** (1996), 149

[12] G. Bressi et al., Nucl. Instr. and Meth. **A396** (1997), 67

[13] S.G. Eckstein, R.H.Pratt, Ann. Phys. (N.Y.) **8** (1959), 297

[14] S. Cerdonio, Doctoral Thesis, Università di Roma "La Sapienza", Italy, 1996 (unpublished).

[15] F. James, MINUIT - Function minimization and error analysis, CERN Program Library D506, 1994

[16] R. Brun et al., GEANT - Detector description and simulation tool, CERN Program library long writeup W5013, 1993

[17] E. Conti et al., Nucl. Instr. and Meth. **A356** (1995), 286

Table 1
Energy-to-ADC counts conversion factor G and electronic noise σ_{sil} of the silicon detectors resulting from the fit of the beam momentum at $p_{beam} = 50.04 MeV/c$.

Silicon number	G (keV/count)	σ_{sil} (keV)
1	1.90	30.
2	1.96	30.
3	2.43	105.
4	1.86	60.
5	1.89	30.
6	1.74	30.

Table 2
Efficiency of each data selection for the experimental data (prompt trigger) ϕ_{exp} and the simulated data ϕ_{MC}. The third column shows the correction factors $f_i = \phi_{exp}/\phi_{MC}$.

Cut number	Cut description	ϕ_{exp}	ϕ_{MC}	Correction factor f_i
1	Silicon overflow	0.993	0.999	0.994
2	Silicon fiducial volume	0.858	0.927	0.926
3	Pion dE/dx	0.958	0.977	0.980
4	$\Delta T_{veto} > \tau_{shap}$	0.553	0.545	1.015
5	$\Delta T_{veto} \leq 3\tau_{\mu}$	0.436	0.804	1.000 (see text)
6	TPC pile-up rejection	0.494	0.824	0.599
7	"synchronous noise" rejection	0.714	0.885	0.808

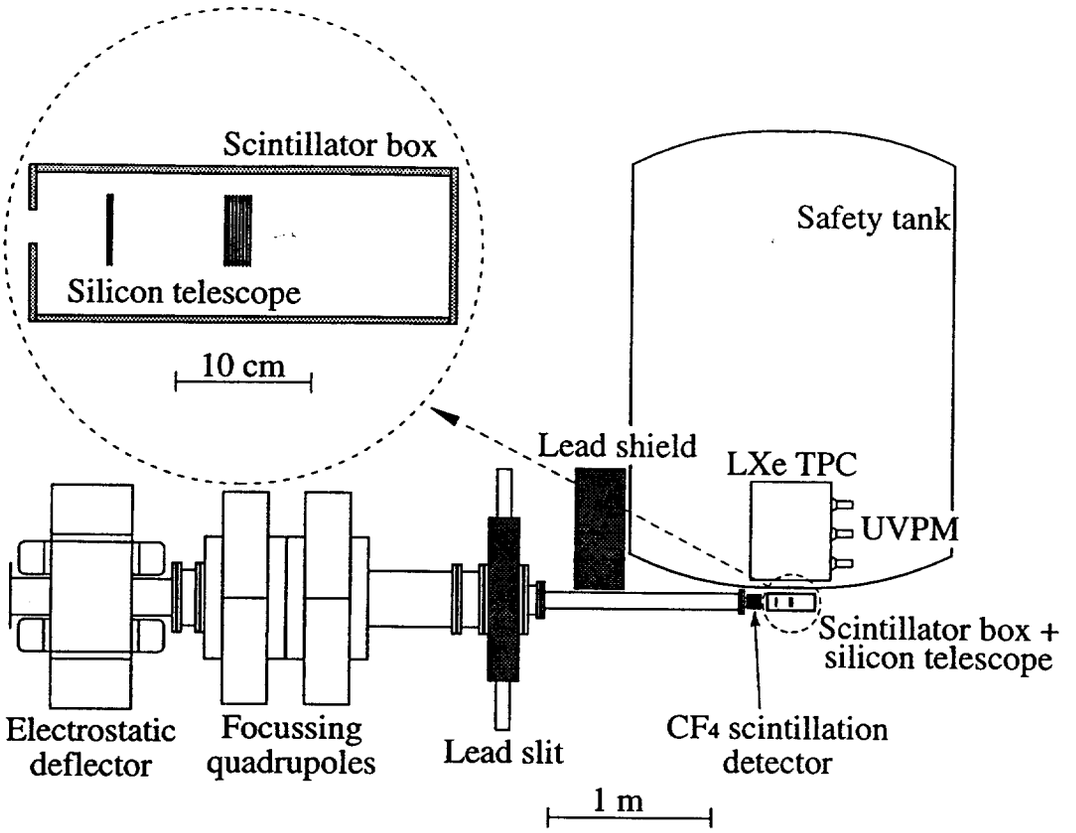

Fig. 1. Layout of the experimental setup.

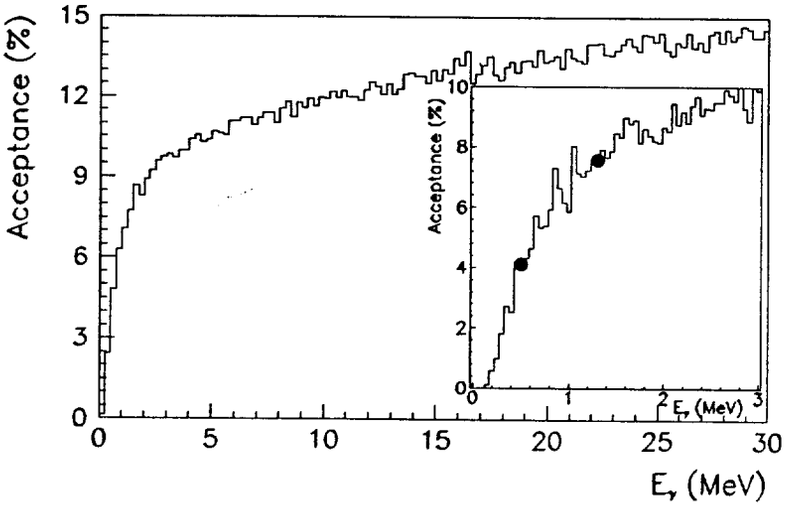

Fig. 2. Total TPC trigger acceptance (from [12]). The two full dots are the experimental measurements (at 511 and 1275 keV) and the histogram shows the MC calculation.

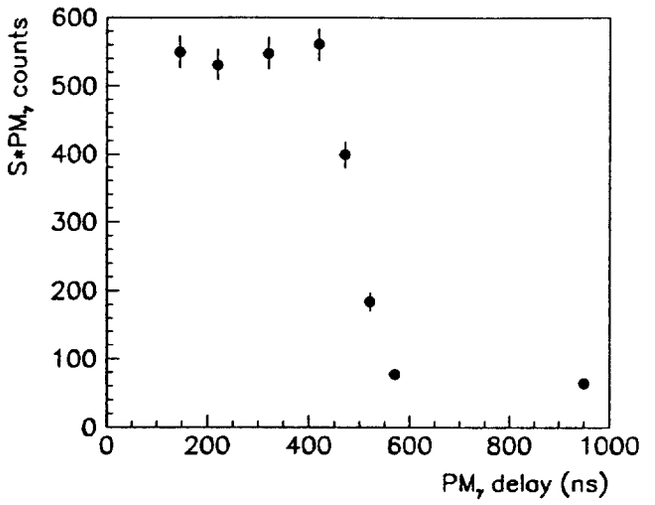

Fig. 3. $S * PM_\gamma$ counts vs. the PM_γ delay.

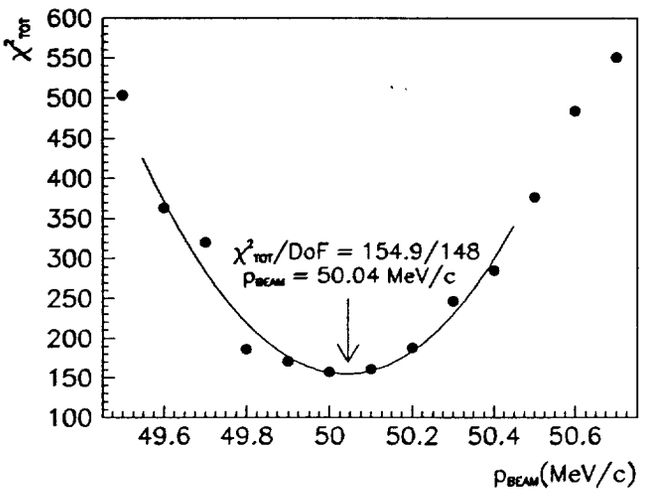

Fig. 4. χ^2_{TOT} vs. p_{beam} from the fit procedure described in the text.

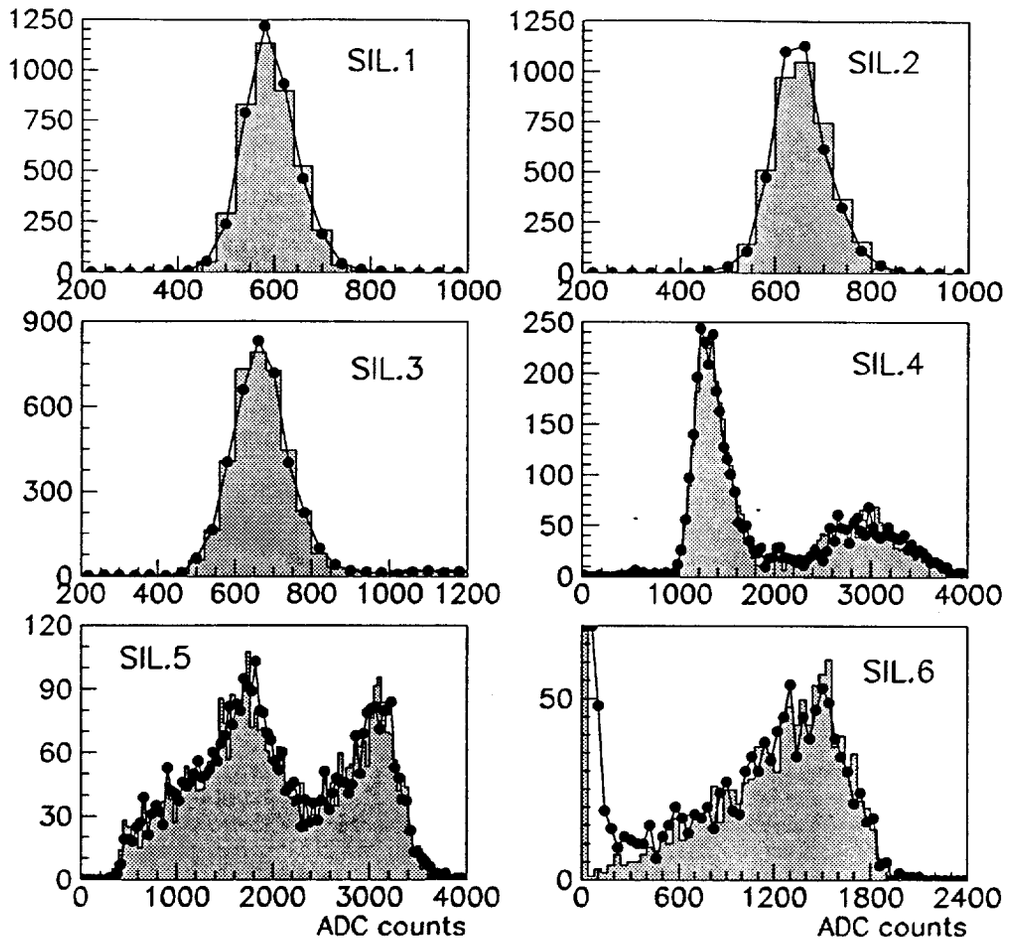

Fig. 5. Spectra of the silicon pads 1-6 for the delayed-data sample (full dots) together with the MC best fit (grey histograms).

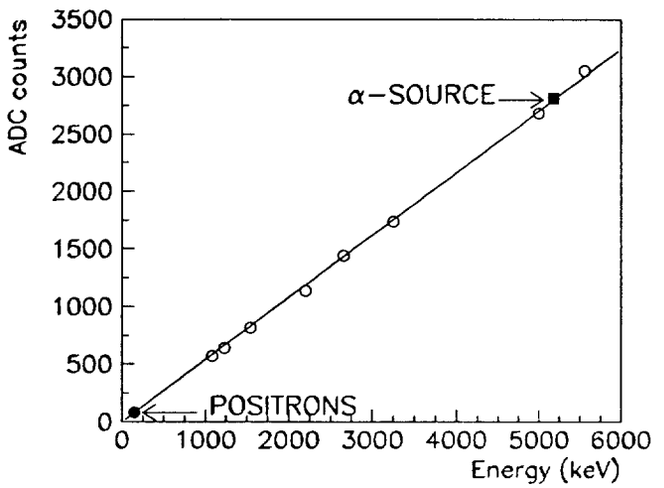

Fig. 6. Dependence of the silicon ADC counts on the energy released. The open circles refer to pions, the full square to the α source and the full dot to positrons.

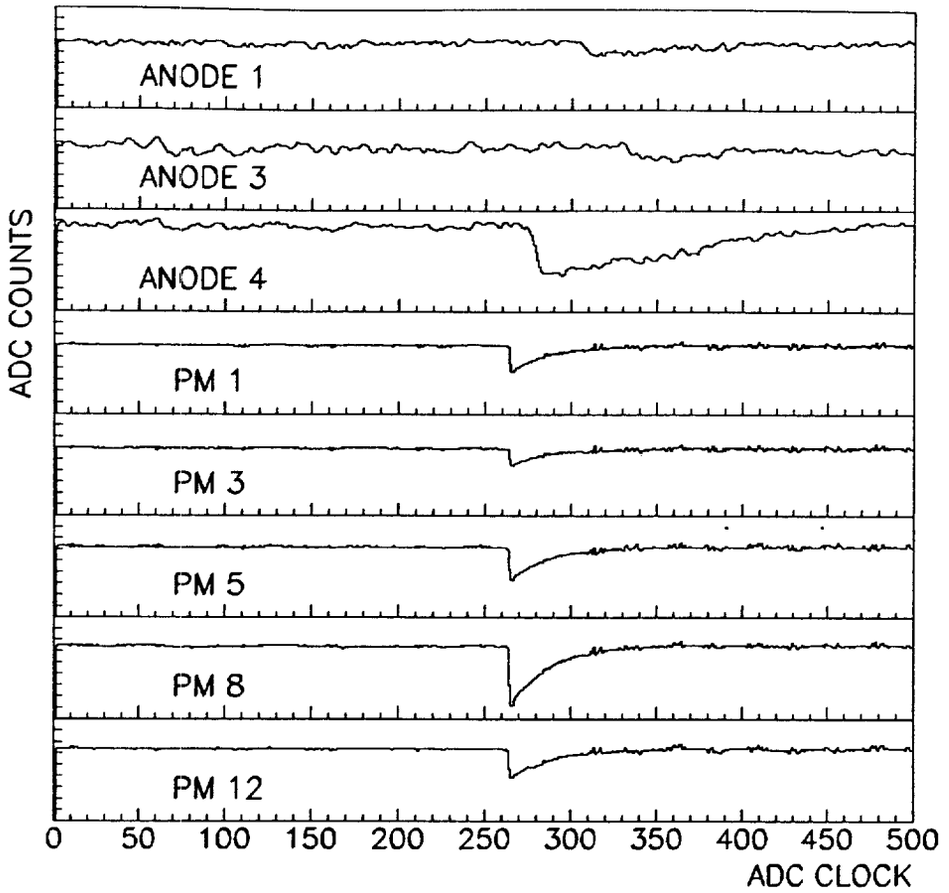

Fig. 7. Example of TPC anode and PM waveforms as they appear at the analysis level. Only the channels with a recognized signal are displayed. The y-scales span 90 ADC counts. The total energy released in the TPC for that event was 2.6 MeV.

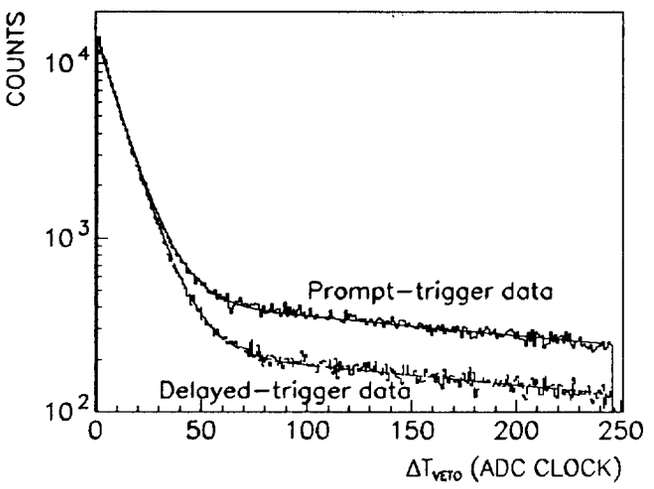

Fig. 8. Distributions of ΔT_{veto} for the prompt-trigger and the delayed-trigger events. The continuous lines are the best fits according to $\Delta T_{veto} = A_1 exp(-t/\tau_1) + A_2 exp(-t/\tau_2)$.

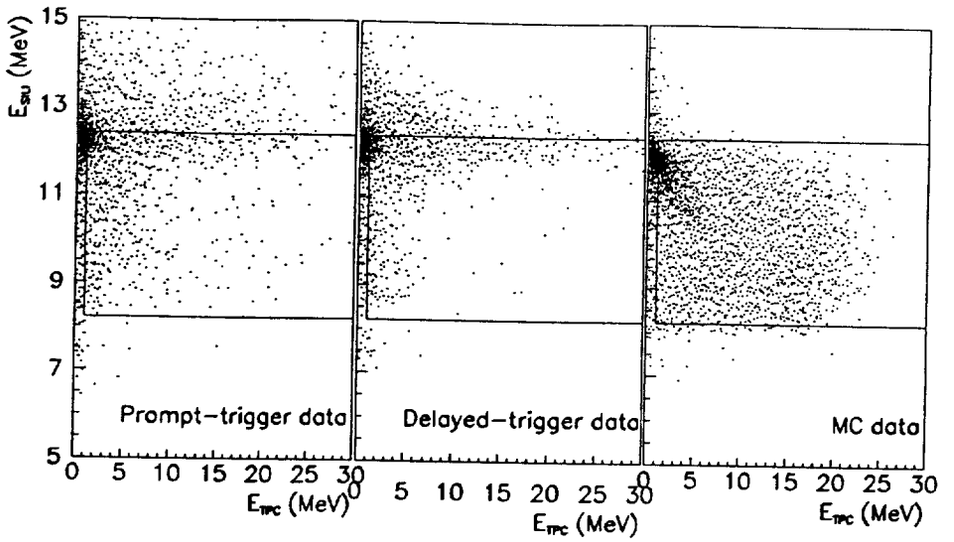

Fig. 9. Dalitz-plot distributions for the prompt-trigger, the delayed-trigger and the MC events after the cuts described in the text. The rectangular contours define the kinematical region where the fit was performed.

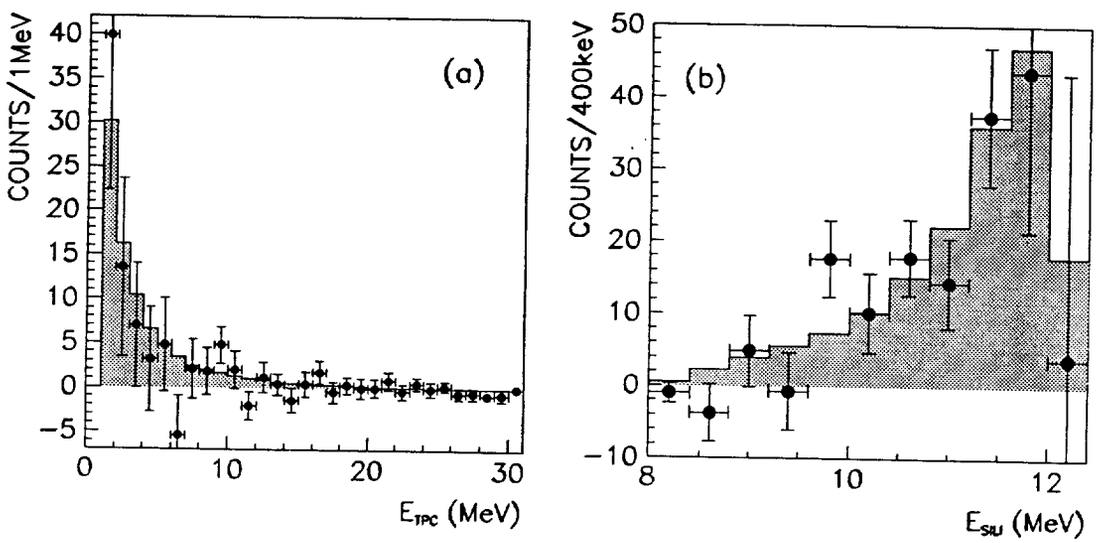

Fig. 10. Spectrum of E_{TPC} (a) and E_{SILI} (b) after background subtraction described in the text. The full dots are the experimental points and the grey histogram the fitted MC distribution.